Structural Color Sensors with Thermal Memory: Measuring Functional Properties of Ti-based Nitrides by Eye

Volker Schnabel,*,† Ralph Spolenak,*,† Max Doebeli,‡ and Henning Galinski†

†*Laboratory for Nanometallurgy, Department of Materials, ETH Zurich, Vladimir-Prelog-Weg 1-5/10, 8093 Zurich, Switzerland*
‡*Ion Beam Physics, ETH Zurich, Otto-Stern-Weg 5, 8093 Zurich, Switzerland*

E-mail: volker.schnabel@mat.ethz.ch; ralph.spolenak@mat.ethz.ch

Abstract

To ensure safe and reliable operation of materials with high thermal loads, e.g. in turbines or thermal solar collectors, it is key to detect material degradation. Here, we present a sensor concept providing a direct optical feedback of thermally induced hardness and resistivity changes in transition-metal-nitride functional coatings. The sensor concept relies on a lossy Gires-Tournois interferometer configuration using thermally induced detuning of a highly absorbing state in the optical spectrum as feedback. We demonstrate for the specific case of TiAlN coatings that such detuning is due to a symmetry-breaking structural phase transition, which is accompanied by the formation of saturated structural colors.

1. Introduction

Every smartphone is equipped with a key set of sensors permanently tracking the ambient temperature, acceleration, air-pressure, humidity and the earth's magnetic field. In fact, smart tracking of critical indicators is fundamental to a plethora of fields, spanning from sports, health care,[1] environmental[2,3] to applied and natural science.[4] Especially, the engineering of nondestructive low footprint monitoring devices based on optics,[5–7] ultrasonics[8] and wearable electronics[9] has attracted a significant interest in research in recent years. Such devices can enable real-time and spatiotemporal tracking of materials properties even in secluded applications, such as offshore wind turbines, or extreme environments, as found in thermal solar collectors.

A state-of-the-art hard-coating material for turbine engines and other applications at high temperatures is TiAlN.[10,11] TiAlN, also used readily in bearings, drills and cutting tools,[12] belongs to the family of transition-metal-nitrides. Compared to TiN, it exhibits superior scratch, wear and oxidation resistance.[13] However, TiAlN is a metastable solid solution, which decomposes into cubic c-TiN and c-AlN at temperatures above 600°C.[14] In an industrial application such thermal instability is highly undesirable, requiring new sensor concepts to promote reliable and safe operation. Here, we design and validate a simple optical sensor platform based on a lossy Gires-Tournois interferometer configuration which is able to track the mechanical and electrical properties of TiAlN at elevated temperatures.

As sensor feedback we use constant detuning of a highly absorbing state in the optical spectrum. In a seminal work Kats *et al.*,[15,16] showed

that such an interferometer design based on a nanometric lossy film on top of a metallic mirror can be utilised to built ultra-thin perfect optical absorbers. In contrast to quarter wave anti-reflection coatings, the optical losses in these absorbers, cause a non-trivial phase shift at the interfaces ($\phi \neq \mod 2\pi$) and allow for ultra-thin layers whose thickness h falls below the "classical" limit of $h = \frac{\lambda}{4n}$.[15,17,18] Still, the total reflectance $R = |\tilde{r}|^2$ of such an absorber is given by the Fresnel equations, namely

$$\tilde{r} = \frac{\tilde{r}_{1,2} + \tilde{r}_{2,3} e^{2i\tilde{\beta}}}{1 + \tilde{r}_{1,2}\tilde{r}_{2,3} e^{2i\tilde{\beta}}} \quad (1)$$

whereby $\tilde{\beta} = (2\pi/\lambda)\tilde{n}_2\delta$, $\tilde{n}_2$ the complex refractive index of the absorbing layer, δ the layer thickness and $\tilde{r}_{1,2}, \tilde{r}_{2,3}$ are the interface specific reflection coefficients.[19] This versatile and simple concept led to a considerable theoretical[17,18] and experimental interest, including research on photovoltaics,[20,21] phase-change materials,[22–24] Janus-faced[25] and other optical coatings.[26–28]

2. Results and Discussion

The principle sensor setup used in this work is illustrated in Figure 1a-c. It combines a thin dielectric TiAlN layer with a metallic mirror made of TiN. Both sensor components were synthesized by magnetron sputtering[29] (see Experimental Section). TiN was selected as it is metallic[30,31] with a resistivity of 16.5 $\mu\Omega$cm corresponding to less than half the resistivity of Ti.[32] In addition, TiN has been established as a temperature-stable plasmonic material with a high melting point of 2930°C in recent years.[33,34] The composition and thickness has been determined using Rutherford backscattering spectrometry (RBS) and X-ray reflectometry (XRR). Detailed information is given in the Supporting Information.

In order to identify a sensor configuration, which is most susceptible to thermally induced changes in refractive index of TiAlN, sensors with different TiAlN coating thickness (12 to 70 nm) have been synthesized. Although only several nanometer thick, the TiAlN coating on TiN severely alters the coupling of light to the structure, manifesting in structural coloration, as shown in Figure 1d. By changing the coating thickness via growth or polishing (Figure 1d) we observe the formation of vivid structural colors spanning from yellow, orange, red, dark and light blue to green. The colors prove to be robust when applied to complex geometry substrates, as demonstrated by depositing on swiss army knife blades (Figure 1d). We characterize the optical response of the sensors for different thicknesses of the dielectric TiAlN layer via near-normal incidence reflectometry. These experiments unveil a resonant absorbing state which manifests in the spectra shown in Figure 1e. The absorbing state red-shifts with increasing TiAlN coating thickness and in the range between $\delta = 24$ to $\delta = 70$ nm the reflectance minimum falls below $R < 5\%$. The experimentally measured spectra are in good agreement with calculated spectra based on Equation 1. The refractive index of TiAlN and TiN has been determined using ellipsometry (Figure S1). Minimum reflectance of 2% is observed for the sensor with a TiAlN thickness of 43 nm at a wavelength of 591 nm. In this thickness regime the attenuation and phase shift accumulation in TiAlN is highly effective and refractive index's variations in the order of 1% can be detected with a simple low-budget spectrometer (see Figure S2).

To quantify the performance of such structures and to effectively detect thermal decomposition in TiAlN coatings, sensors with $\delta = 24, 43$ and 70 nm have been annealed between 400 and 900°C in steps of 100°C. The pseudocolor plots in Figure 2a show the measured reflectance of the TiAlN-TiN films as a function of annealing temperature. The corresponding change in structural coloration is shown alongside. For all configurations the spectral position of the absorbing state, i.e. minimal reflectance, blueshifts as function of temperature. This effect is result of the decreasing refractive index n_{TiAlN} as the position of the reflectance minimum scales with $\lambda_{\min} \propto n_{\mathrm{TiAlN}} \cdot \delta$. To this extent, the thermally induced changes can be

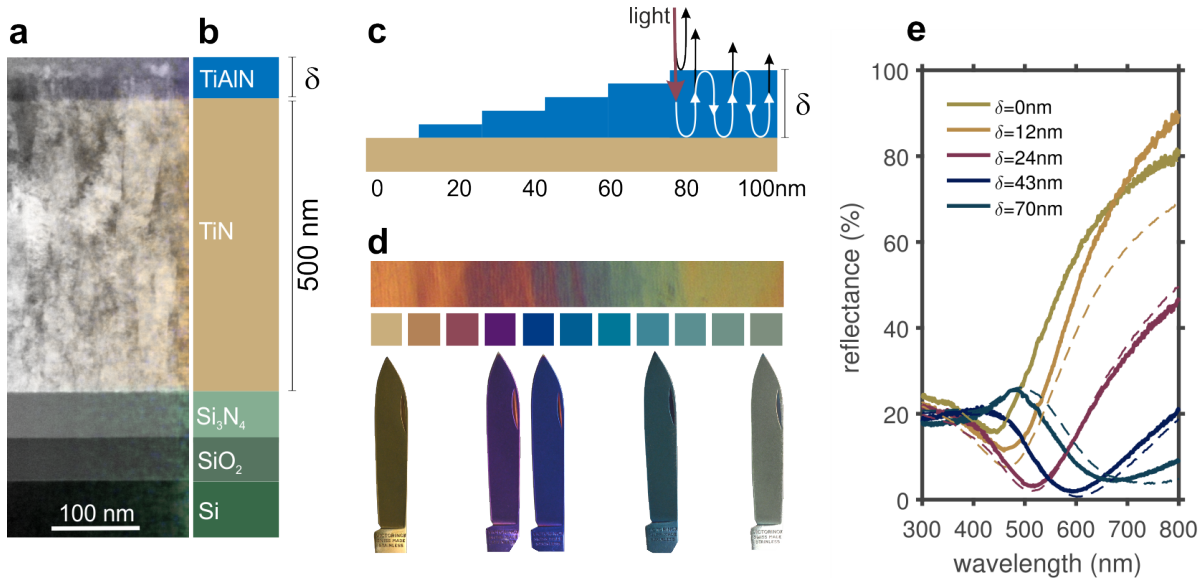

Figure 1: Morphology and structural color of TiAlN-TiN absorbers. a) Dark field scanning electron transmission electron microscopy image with an energy-dispersive X-ray spectroscopy elemental distribution map overlay of the strong interference resonator in cross-section. b) Schematic of a strong interference resonator. c) TiAlN-TiN sensor concept based on a lossy Gires-Tournois interferometer configuration. d) Optical micrograph of an intentionally obliquely polished resonator (top). TiAlN thickness before polishing was 500 nm. Due to the oblique polishing, the TiAlN thickness to the right is about 100 nm, whereas the TiAlN coating is fully removed to the left revealing the TiN coating deposited underneath. Predicted TiAlN thickness dependent color evolution according to Equation 1 (middle) and strong interference resonators with TiAlN thicknesses ranging from 0 to 100 nm deposited on stainless steel knife blades (bottom). e) Measured and calculated reflectance using Equation 1 as a function of wavelength, within the range of 300 to 800 nm as solid and dashed lines, respectively.

understood as decrease in optical thickness (see Figure S3), which reverses the structural coloration observed in Figure 1d. To analyze in more detail the mechanism behind the thermal detuning of the absorbing state, it has to be considered that TiAlN is a metastable solid solution, which upon thermal activation phase separates.[14] This process is schematically illustrated in Figure 2b and 2c. In the initial state (Figure 2b) TiAlN exhibits a random distribution of Ti and Al on the metallic sub-lattice.[35] Upon annealing, TiAlN phase separates in c-TiN and c-AlN rich domains[14,35] leading to an ordering on the metallic sub-lattice (Figure 2c). The ordering causes an increase in Ti-Ti next-nearest-neighbor bond fraction giving rise to an increased fraction of hybridized Ti-Ti *d* electronic states.[36] When we normalize the shift of reflectance minimum by the coating thickness, we observe a behavior charateristic for a second-order phase transition with a critical transition temperature of $T_c = 694°C$ as shown in Figure 3d. This result is very important as it indicates that we can treat the phase separated TiAlN as an effective medium and that the optical response is unaffected by changes in sensor architecture.

Quite interestingly, the found phase transition can be traced back to specific oscillators within a Drude-Lorentz model describing the permittivity of TiAlN as function of annealing temperature. These oscillators show the same universal scaling behavior typically found for phase transitions in a 2D-Ising model (see Supporting Information).

To experimentally verify the effective medium approach and for further insight into the thermally induced structural, mechanical and elec-

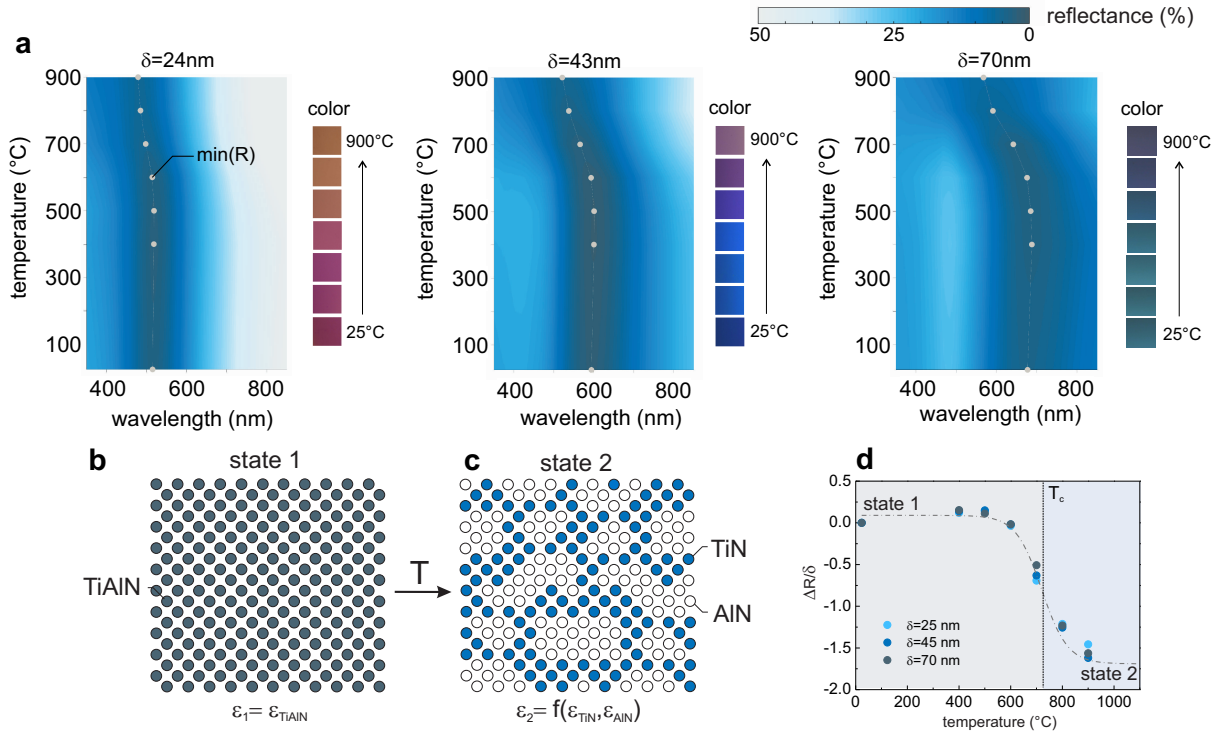

Figure 2: Evaluation of thermally induced evolution in optical properties of TiAlN-TiN strong interference resonators. a) Reflectance as a function of annealing temperature for TiAlN film thicknesses of 24, 43 and 70 nm. b) Schematic of TiAlN decomposition process from a solid solution (state 1) to a in c) illustrated self-organized structure of TiN rich and AlN rich domains (state 2). d) TiAlN thickness normalized reflectance shift as a function of annealing temperature.

trical evolution of TiAlN, we employ a correlative X-ray diffraction (XRD), high-resolution transmission electron microscopy (TEM) approach. Figure 3a shows X-ray diffraction analysis in the 2-Theta range from 34 to 40°. The appearance of the shoulder to the left of the main peak at temperatures > 700°C and the decrease in intensity of the main peak indicates the phase separation into c-TiN enriched and c-AlN enriched domains.[14,35,37] To evaluate the domain size of the phase separated TiAlN thin film, we use high-resolution TEM. Figure 3b and 3c show a cross-section TEM micrograph of a sensor composed of a 43 nm thick TiAlN layer on 500 nm TiN, which was annealed at 900°C. We identify the different phases of the material of a selected region in Figure 3c by calculating the corresponding diffraction pattern using a fast Fourier transform (FFT). As highlighted by blue and red circles in Figure 3e, the diffraction pattern confirms AlN enriched and TiN enriched c-TiAlN (200) domains. By calculating the inverse FFT of a specific AlN diffraction spot, we can visualize AlN rich domains (see Figure 3d). The characteristic domain size d is in the order of 5 nm, confirming, the highly subwavelength nature ($d << \lambda$).

To experimentally demonstrate that the thermal detuning of the absorbing state can be used to sense changes in other materials properties, we measured the hardness and resistivity of TiAlN for different annealing temperatures. Both materials properties shown in Figure 3f and 3e respectively, show characteristic behavior indicative of a structural phase transition. However, while the hardness increases due to thermally induced age hardening,[14] the resistivity decreases due to a shift towards a higher fraction of metallic Ti-Ti next-nearest-neighbour bonds.[32,38] We note that when looking at the resistivity the critical temperature of the transition is reduced. This effect can be un-

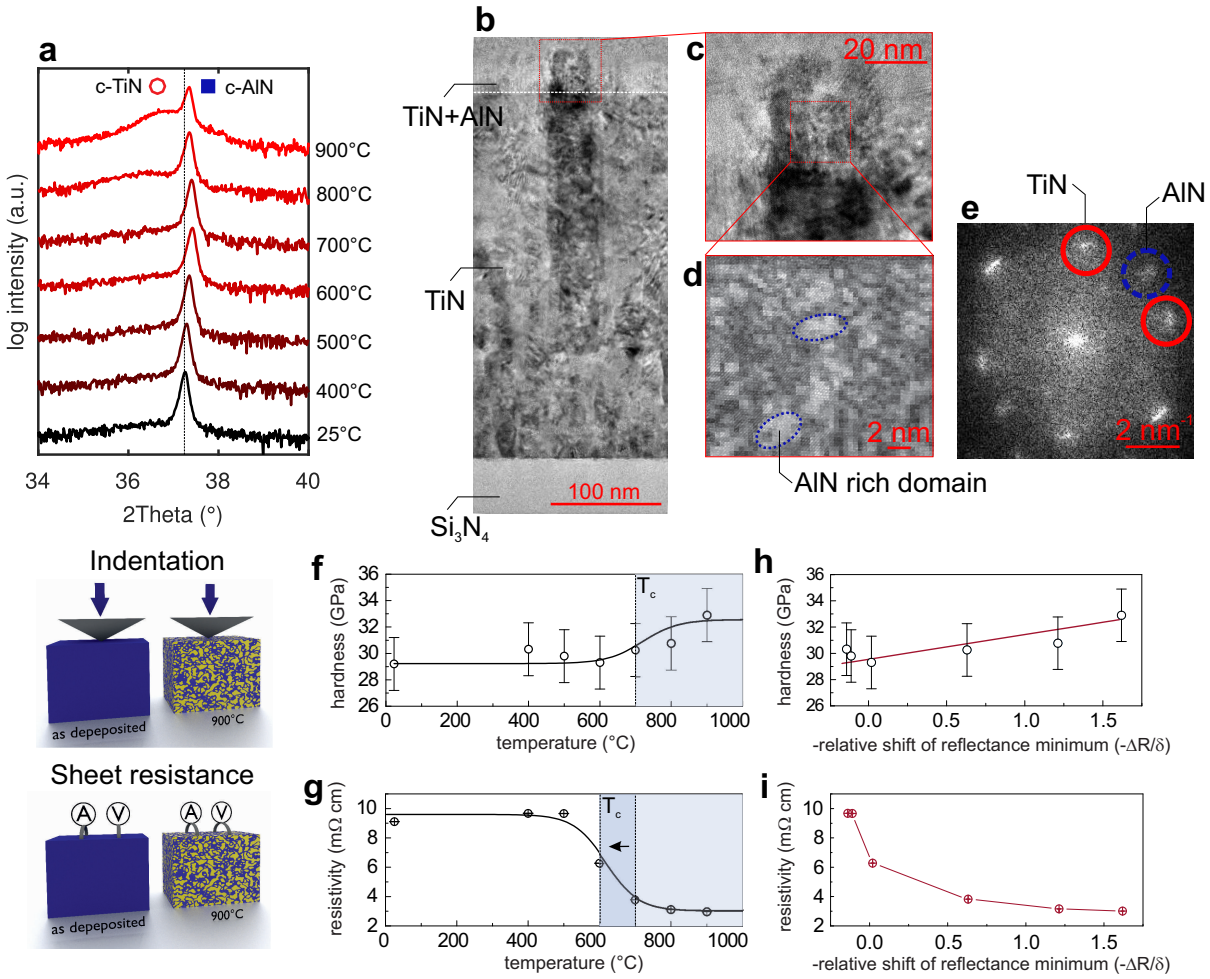

Figure 3: Microstructural, mechanical and electrical analysis of TiAlN thin films. a) X-ray diffraction analysis from 34 to 40° 2-Theta within the temperature range of 25 to 900°C. Intensities are displayed on a logarithmic scale. b) Cross-sectional TEM micrograph of a TiAlN-TiN strong interference resonator with a TiAlN film thickness of 43 nm annealed at 900°C. c) Magnified TEM micrograph from the TiAlN top layer. d) Overlay of a high-resolution TEM micrograph with a reverse Fourier transform from the area highlighted in c). e) Diffraction spots highlighted by blue and red circles corresponding to distances in agreement with c-AlN and c-TiN (200) lattice planes. f) Nanoindentation hardness evolution of a 500 nm thick TiAlN film on Si as a function of annealing temperature. g) Resistivity of a 500 nm thick TiAlN film on Si as a function of annealing temperature. h) Observed relation between hardness of TiAlN and thickness normalized relative shift of reflectance minimum. i) Observed relation between resistivity of TiAlN and thickness normalized relative shift of reflectance minimum.

derstood in terms of percolation theory, as only one percolating conducting Ti-Ti bond path is sufficient to change the materials resistivity.[39] By relating the thermally induced changes in hardness and resistivity to the optical feedback given by the relative shift of reflectance minimum, we retrieve the sensor response. The corresponding calibration curves relating hardness and resistivity to the optical feedback are shown in Figure 3h and 3i. Both properties change as a function of the system's optical feedback confirming that the detuning of the absorbing state can serve as fingerprint for these functional properties under a thermal load.

3. Conclusions

We have experimentally demonstrated a new sensor concept to directly measure the thermally induced hardness and resistivity changes in TiAlN coatings, a state-of-the-art coating material in turbines.[40] Embedding this material in a lossy Gires-Tournois interferometer configuration enables tracking of the thermally induced phase separation accompanied by an increase in fraction of hybridized Ti-Ti *d*-bonds. The changes in electronic symmetry cause detuning of an absorbing state in the optical spectrum. This absorbing state can be altered via thermal treatment resulting in the formation of temperature-dependent structural coloration. We show that displacement of the absorbing state is directly related to changes in hardness and resistivity in the material.
The presented sensor can be used in high temperatures (1000°C) and enables the continuous detection of changes in refractive index $> 1\%$. The sensor concept can be easily adapted to other applications, opening up new possibilities for engineering low footprint sensor devices, capable to detect and track local property changes of materials and devices in real-time. These sensors are ideal for application in secluded locations, such as offshore wind turbines, or in extreme environments as in solar collectors.

4. Experimental Section

TiN and TiAlN layers were synthesized by reactive magnetron sputtering from elemental targets with a purity larger than 99.99%. For the deposition direct current power supplies were run in power controlled mode with power densities of 15 and 7.5 W/cm^2 for Ti and Al, respectively. The base pressure was lower than 1.3×10^{-4} Pa. We employed an Ar/N_2 gas mixture of 10/1 and 5/1 for the deposition of TiN and TiAlN, respectively. The working pressure was set to 0.4 Pa. The substrates were intentionally heated to 400°C and a negative bias potential of 100 V was applied. Thickness, density and roughness of the thin films were analyzed by X-ray reflectivity, utilizing a PANalytical Xpert^3 MRD platform equipped with a Cu source, an X-ray mirror and a parallel plate collimator. Refractive indices were measured with an ellipsometer at incidence angles of 66 to 74°. The phase difference and amplitude component were fitted by the Cauchy equation. Reflectance measurements were conducted at near zero angle with a fiber spectrometer. TEM lamellas were prepared using a focused ion beam (FIB-SEM) dual-beam station (Zeiss NVision40) operating with a Ga^+ source at 30 and 5 kV. TEM was conducted at a FEI Talos F200X system equipped with SuperX EDS-STEM detectors. Hardness measurements were conducted with a depth-sensing nanoindenter (Hysitron TriboIndenterTM) equipped with a Berkovich tip. The maximum contact load was adjusted for a contact-depth of less than 10% of film thickness.[41] Sheet resistance was measured employing the Van der Pauw method[42] using a Keysight B2962A power supply. RBS measurements were performed with a 2 MeV ^{4}He beam and a Si PIN diode detector under 168° scattering angle. The N/O ratio was determined by heavy ion elastic recoil detection using a 13 MeV ^{127}I beam with a combination of a time-of-flight and a gas ionization detector.[43]

Acknowledgement

V.S. conceived the concept; V.S. and H.G. designed the research; V.S. conducted synthesis and experimental characterization; V.S. and H.G. analyzed the data; H.G conducted the modelling and optical calculations; M.D. performed the RBS measurements; V.S and H.G wrote the manuscript; R.S provided conceptual advice and critically reviewed the manuscript. The authors thank the Scientific Center for Optical and Electron Microscopy (ScopeM), the Department of Materials X-ray platform and the FIRST cleanroom team at the ETH Zurich for their support. H. G. gratefully acknowledges financial support from the Size Matters! project, (TDA Capital, UK).

References

(1) Gravitz, L. *Nature* **2016**, *538*, S8.

(2) Brewin, R. J. W.; de Mora, L.; Jackson, T.; Brewin, T. G.; Shutler, J. *PLOS ONE* **2015**, *10*, 1–22.

(3) Wang, W.; Kennedy, R.; Lazer, D.; Ramakrishnan, N. *Science* **2016**, *353*, 1502–1503.

(4) Viti, L.; Hu, J.; Coquillat, D.; Politano, A.; Consejo, C.; Knap, W.; Vitiello, M. S. *Advanced Materials* **2016**, *28*, 7390–7396.

(5) Zobenica, A.; van der Heijden, R. W.; Petruzzella, M.; Pagliano, F.; Leijssen, R.; Xia, T.; Midolo, L.; Cotrufo, M.; Cho, Y.; van Otten, F. W. M.; Verhagen, E.; Fiore, A. *Nature Communications* **2017**, *8*, 2216–.

(6) Shillingford, C.; Russell, C. W.; Burgess, I. B.; Aizenberg, J. *ACS Applied Materials & Interfaces* **2016**, *8*, 4314–4317, PMID: 26854914.

(7) Majumder, M.; Gangopadhyay, T. K.; Chakraborty, A. K.; Dasgupta, K.; Bhattacharya, D. *Sensors and Actuators A: Physical* **2008**, *147*, 150 – 164.

(8) Di Sante, R. *Sensors* **2015**, *15*, 18666–18713.

(9) Kim, J.; Kim, M.; Lee, M.-S.; Kim, K.; Ji, S.; Kim, Y.-T.; Park, J.; Na, K.; Bae, K.-H.; Kyun Kim, H.; Bien, F.; Young Lee, C.; Park, J.-U. *Nature Communications* **2017**, *8*, 14997.

(10) Hakansson, G.; Sundgren, J.; McIntyre, D.; Greene, J.; Münz, W. *Thin Solid Films* **1987**, *153*, 55 – 65.

(11) Rachbauer, R.; Gengler, J. J.; Voevodin, A. A.; Resch, K.; Mayrhofer, P. H. *Acta Materialia* **2012**, *60*, 2091 – 2096.

(12) Chim, Y.; Ding, X.; Zeng, X.; Zhang, S. *Thin Solid Films* **2009**, *517*, 4845 – 4849.

(13) Münz, W.-D. *Journal of Vacuum Science & Technology A: Vacuum, Surfaces, and Films* **1986**, *4*, 2717–2725.

(14) Mayrhofer, P. H.; Hörling, A.; Karlsson, L.; Sjölen, J.; Larsson, T.; Mitterer, C.; Hultman, L. *Applied Physics Letters* **2003**, *83*, 2049–2051.

(15) Kats, M. A.; Blanchard, R.; Genevet, P.; Capasso, F. *Nature Materials* **2013**, *12*, 20–24.

(16) Kats, M. A.; Capasso, F. *Laser & Photonics Rev.* **2016**, *10*, 699–699.

(17) Rensberg, J.; Zhou, Y.; Richter, S.; Wan, C.; Zhang, S.; Schöppe, P.; Schmidt-Grund, R.; Ramanathan, S.; Capasso, F.; Kats, M. A.; Ronning, C. *Phys. Rev. Applied* **2017**, *8*, 014009.

(18) Park, J.; Kim, S. J.; Brongersma, M. L. *Opt. Lett.* **2015**, *40*, 1960–1963.

(19) BORN, M.; WOLF, E. In *Principles of Optics (6^{th} EDITION)*, sixth (corrected) edition ed.; BORN, M., WOLF, E., Eds.; Pergamon, 1980; pp 611 – 664.

(20) Lee, K.-T.; Lee, J. Y.; Seo, S.; Guo, L. J. *Light: Science &Amp; Applications* **2014**, *3*, e215.

(21) Li, Q.; Du, K.; Mao, K.; Fang, X.; Zhao, D.; Ye, H.; Qiu, M. *Scientific Reports* **2016**, *6*, 29195.

(22) Bakan, G.; Ayas, S.; Saidzoda, T.; Celebi, K.; Dana, A. *Applied Physics Letters* **2016**, *109*, 071109.

(23) Kats, M. A.; Sharma, D.; Lin, J.; Genevet, P.; Blanchard, R.; Yang, Z.; Qazilbash, M. M.; Basov, D. N.; Ramanathan, S.; Capasso, F. *Applied Physics Letters* **2012**, *101*, 221101.

(24) Schlich, F. F.; Zalden, P.; Lindenberg, A. M.; Spolenak, R. *ACS Photonics* **2015**, *2*, 178–182.

(25) England, G. T.; Russell, C.; Shirman, E.; Kay, T.; Vogel, N.; Aizenberg, J. *Advanced Materials* **2017**, *29*, 1606876–n/a, 1606876.

(26) Schlich, F. F.; Spolenak, R. *Applied Physics Letters* **2013**, *103*, 213112.

(27) Ji, C.; Lee, K.-T.; Xu, T.; Zhou, J.; Park, H. J.; Guo, L. J. *Advanced Optical Materials* **2017**, *5*, 1700368–n/a, 1700368.

(28) Mirshafieyan, S. S.; Guo, J. *Opt. Express* **2014**, *22*, 31545–31554.

(29) Schnabel, V.; Sologubenko, A. S.; Danzi, S.; Kurtuldu, G.; Spolenak, R. *Applied Physics Letters* **2017**, *111*, 173902.

(30) Patsalas, P.; Logothetidis, S. *Journal of Applied Physics* **2001**, *90*, 4725–4734.

(31) Lalisse, A.; Tessier, G.; Plain, J.; Baffou, G. *Scientific reports* **2016**, *6*, 38647.

(32) Münster, A.; Sagel, K.; Schlamp, G. *Nature* **1954**, *174*, 1154.

(33) Chirumamilla, M.; Chirumamilla, A.; Yang, Y.; Roberts, A. S.; Kristensen, P. K.; Chaudhuri, K.; Boltasseva, A.; Sutherland, D. S.; Bozhevolnyi, S. I.; Pedersen, K. *Advanced Optical Materials* **2017**, *5*, 1700552.

(34) Reddy, H.; Guler, U.; Kudyshev, Z.; Kildishev, A. V.; Shalaev, V. M.; Boltasseva, A. *ACS Photonics* **2017**, *4*, 1413–1420.

(35) to Baben, M.; Hans, M.; Primetzhofer, D.; Evertz, S.; Ruess, H.; Schneider, J. M. *Materials Research Letters* **2017**, *5*, 158–169.

(36) Alling, B.; Ruban, A. V.; Karimi, A.; Peil, O. E.; Simak, S. I.; Hultman, L.; Abrikosov, I. A. *Phys. Rev. B* **2007**, *75*, 045123.

(37) Petrov, I.; Hultman, L.; Helmersson, U.; Sundgren, J.-E.; Greene, J. *Thin Solid Films* **1989**, *169*, 299 – 314.

(38) Wahlström, U.; Hultman, L.; Sundgren, J.-E.; Adibi, F.; Petrov, I.; Greene, J. *Thin Solid Films* **1993**, *235*, 62 – 70.

(39) Reuteler, J.; Hütter, M.; Gauckler, L. J. *Journal of Applied Physics* **2011**, *110*, 024909.

(40) Doell, A. Oerlikon Balzers announces BALINIT TURBINE PRO, the coating solution for turbine blades. 2017; `https://www.oerlikon.com/balzers/com/en/service-area/press/press-releases-detail/128894/`.

(41) Oliver, W.; Pharr, G. *J. Mater. Res.* **1992**, *7*, 1564–1583.

(42) der Pauw, L. V. *Philips Research Reports* **1958**, *13*, 1–9.

(43) M. Nastasi, J. M.; Wang, Y. *Ion Beam Analysis*; CRC Press, 2015.